We are IntechOpen,
the world's leading publisher of
Open Access books
Built by scientists, for scientists

4,800
Open access books available

122,000
International authors and editors

135M
Downloads

Our authors are among the

154
Countries delivered to

TOP 1%
most cited scientists

12.2%
Contributors from top 500 universities

BOOK CITATION INDEX
CLARIVATE ANALYTICS
INDEXED

WEB OF SCIENCE™

Selection of our books indexed in the Book Citation Index
in Web of Science™ Core Collection (BKCI)

Interested in publishing with us?
Contact book.department@intechopen.com

Numbers displayed above are based on latest data collected.
For more information visit www.intechopen.com

Chapter

Heat and Mass Transfer in Outward Convex Corrugated Tube Heat Exchangers

Huaizhi Han, Bingxi Li, Yaning Zhang, Quan Zhu and Ruitian Yu

Abstract

Heat and mass transfer in outward convex corrugated tube heat exchangers is of significant importance for the optimization, fabrication, and application of outward convex corrugated tube heat exchangers. This chapter gives a deep investigation of the heat and mass transfer in outward convex corrugated tube heat exchangers. Based on the experimental setup developed, the performances of a novel outward convex corrugated tube heat exchanger are presented. Simulation methods are then used to detail the heat and mass transfer at tube side and shell side of the outward convex corrugated tube heat exchanger, and these include the flow structure, temperature distribution, and turbulence kinetic energy. Heat and mass transfer enhancements of the outward convex corrugated tube heat exchanger are also studied, and they are from tube side, shell side, and overall system aspects. Finally, multi-objective optimization of the outward convex corrugated tube heat exchanger is conducted to obtain the optimal performances through using Response Surface Methodology (RSM) and Non-dominated Sorting Genetic Algorithm (NSGA-II). Main conclusions and future outlook are then briefly stated and summarized. We firmly believe that the contents presented in this chapter can not only enrich the knowledge of heat exchangers but also develop methods for studying heat exchangers.

Keywords: heat and mass transfer, heat exchanger, outward convex corrugated tube, enhancement, optimization

1. Introduction

The outward convex corrugated tube heat exchanger (CTHE) is a novel kind of shell and tube heat exchangers, which can be applied in many applications. Designing this kind of heat exchangers is considerable flexibility because the geometrical structure can be varied easily by altering the tube diameter, length, and arrangement [1, 2]. The exchanger can be designed for suffering high pressure condition. The exchangers are applied primarily for single phase and phase change heat transfer application. They could also be used for heat transfer applications with high operating temperature and/or pressure.

Figure 1 shows a bundle of outward convex corrugated tubes (CT) fabricated in the tubesheets, which is the most significant components in the CTHE. Two kinds of
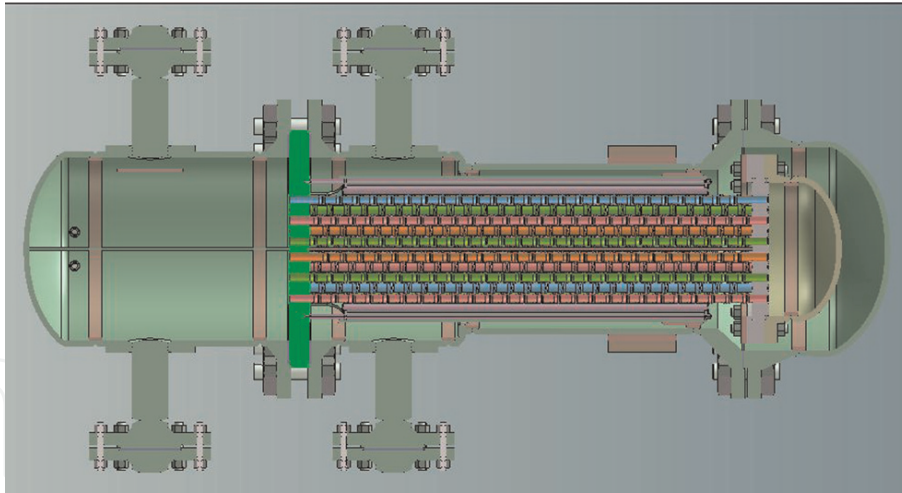
Figure 1.
The schematic of out outward convex corrugated tube heat exchangers.

fluids flow inside and outside of CT, respectively. Except the tube bundles, the major components of this exchanger also include shell, front-end head, and rear-end head.

The exchangers could be widely used in industry for the following reasons. (a) Wide capacity and operating conditions, such as from high vacuum to ultrahigh pressure (over 100 MPa) and from cryogenics to high temperatures (about 1100°C). (b) Special operating conditions: vibration, heavy fouling, highly viscous fluids, erosion, corrosion, toxicity, radioactivity, multicomponent mixtures, and so on. (c) The most versatile exchangers, made from a variety of metal and nonmetal materials (such as graphite, glass, and Teflon) and range in size from small to supergiant surface area. (d) Extensively applications: petroleum-refining and chemical industries; as steam generators, condensers, boiler feedwater heaters, and oil cooler in power plants; as condensers and evaporators in some air-conditioning and refrigeration applications; in waste heat recovery applications; and in environmental control [3–5].

The main difference between the CTHE and traditional heat exchangers is the adopted tube type. Traditionally, the inward intermittent or continuous type corrugated tubes are employed, as an example for both helically corrugated and transverse corrugated tubes, owing to their ease of realization. However, in engineering devices, it is necessary to adopt CT, which could be conveniently and periodically inspected with complete accessibility [6].

A schematic view of the CT configuration currently investigated is shown in **Figure 2**. The structure parameters of the outward corrugated tube include inner diameter (D), tube length (L), corrugation height (H), corrugation pitch (p), corrugation crest radius (R), and corrugation trough radius (r).

The design and improvement of the CT are considered a significant aspect of researches in terms of heat and mass transfer. Almost all of the heat transfer augmentation techniques have been introduced to improve the overall thermo-hydraulic performance. Thus, these techniques achieved reductions in the size and cost of heat exchangers.

2. Performances of outward convex corrugated tube heat exchangers

2.1 Manufacture of corrugated tube heat exchangers

Manufacture consideration could be divided into manufacturing equipment, processing, and other qualitative criteria. The equipment considerations determine
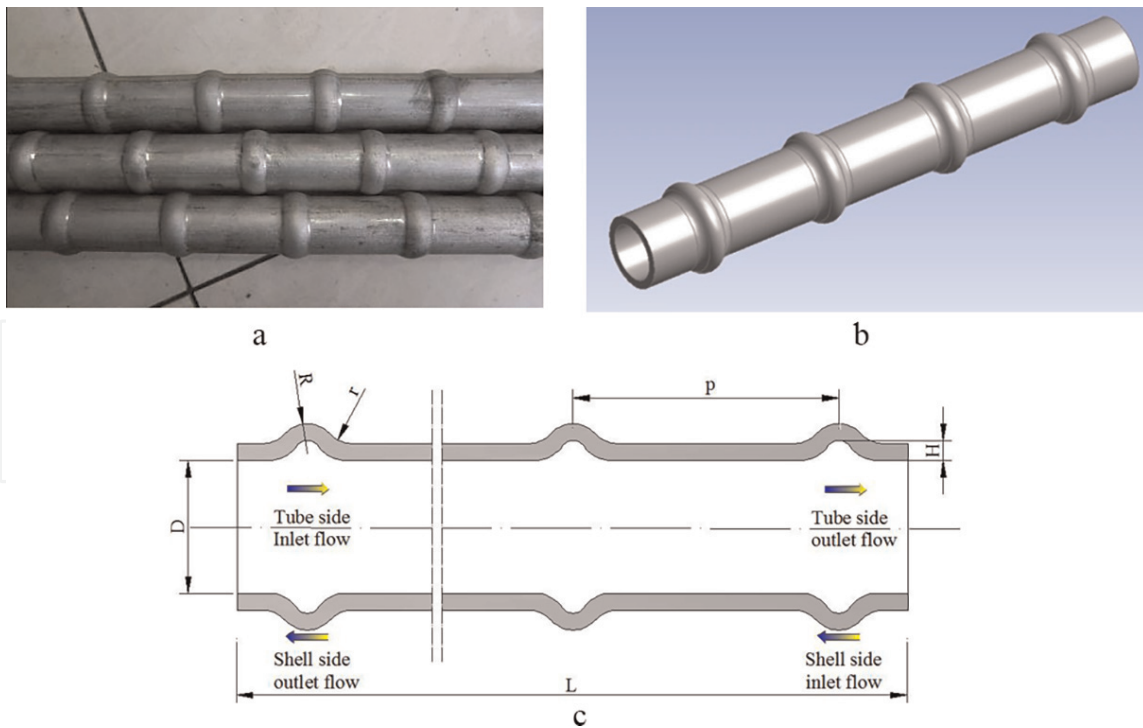
Figure 2.
The real and schematic view of the outward convex corrugated tube.

which design could be selected, which include existing and new tooling, availability and limitations of equipment, offline production, and investment funding. Processing considerations make sure how individual parts and components of a heat exchanger are manufactured and assembled, which including manufacture of individual parts, stacking of a heat exchanger core and eventual brazing, mounting of pipes, washing/cleaning of the exchanger, and leak testing in the system. When a heat exchanger is designed, the manufacturing equipment and the complete processing considerations must be evaluated previously, particularly for an extended surface heat exchanger [11, 12].

In the novel tube and shell heat exchanger, the structure of the outward convex corrugated tube is special, composed of alternating corrugated segment and straight pipe section. The main difference from traditional heat exchanger is the adopted structure, so the manufacture processing for the novel tube type is highlighted in this section. The working conditions of the heat exchanger are mainly for high temperature and pressure operation condition. To ensure the safe operation of heat exchanger, a thick-walled stainless steel tube with strong pressure resistance is selected as the base tube. For example, the mechanical properties of stainless steel tube material are as follows: yield strength is 390 MPa, material hardening index is 0.148, material strength coefficient is 764 MPa, material anisotropy coefficient is 0.83, material modulus of elasticity is 207GPa, and Poisson ratio is 0.28.

The outward convex corrugated tube is manufactured according to high pressure hydraulic bulking based on the smooth stainless steel tube. The hydraulic bulking equipment is 10,000 KN. As shown in **Figure 3(a)**, the equipment is assembled with 400 MPa internal high-pressure forming system, which is mainly composed of the supercharger, two horizontal push cylinder hydraulic servo system, and computer control system. The manufacturing process needs to be supplemented with the corresponding mold, installed on the hydraulic bulking equipment. The mold consists of three parts, which includes upper module as shown in **Figure 3(b)**, lower module as shown in **Figure 3(c)** and sealing punch. The inner mosaic block with corrugation shape is inserted in the mold as shown in
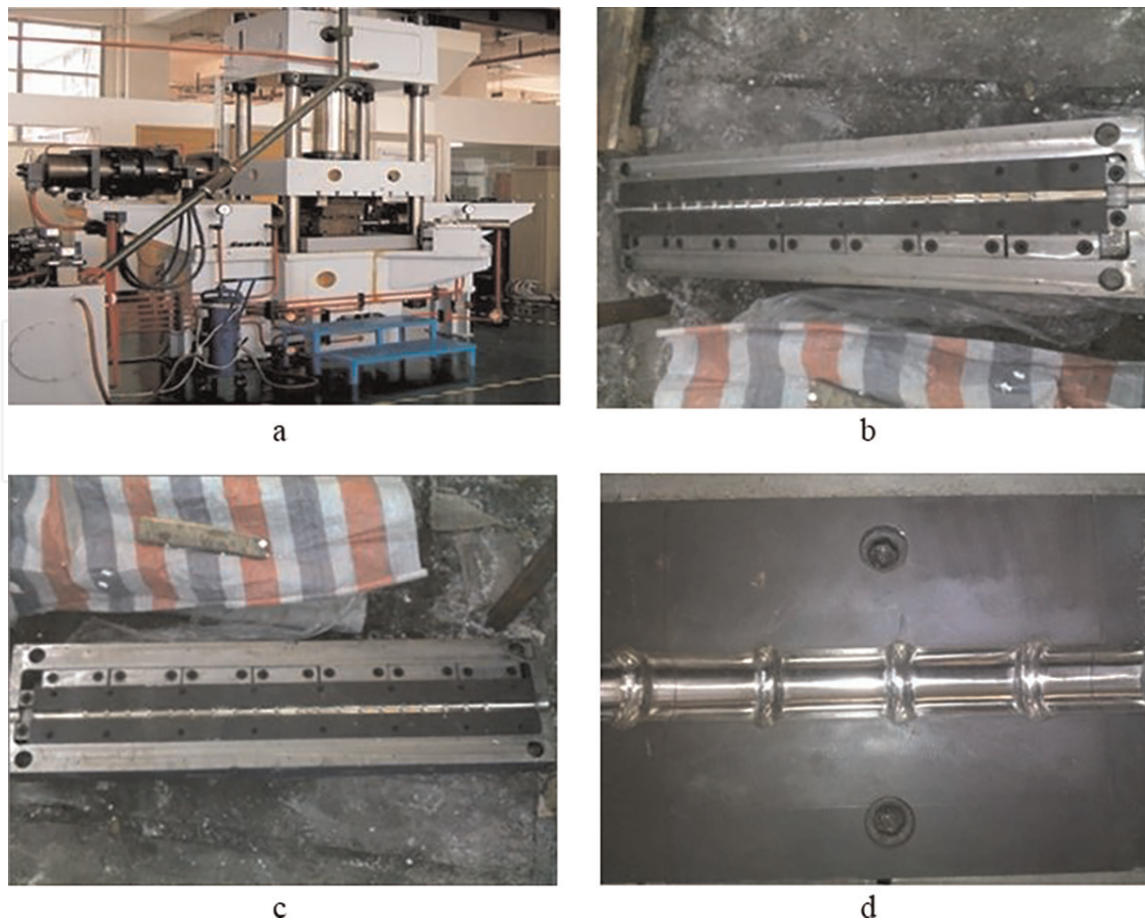
Figure 3.
The hydraulic bulging machine and mold. Based on the modified order as the above sticky. (a) Hydraulic bulking equipment; (b) upper module; (c) lower module; (d) inner mosaic block.

Figure 3(d). High pressure liquid (water or oil) is provided inside the smooth stainless steel tube and finally hydroforms the outward convex corrugated tube.

2.2 Layout of corrugated tube heat exchangers

In order to test the heat transfer and resistance performance of the corrugated tube heat exchangers, experimental study on the corrugated tube heat exchanger must be performed. We adopted steady-state techniques to establish the relationship between *Nu* and *Re*. Different data acquisition and reduction methods are used, depending on whether the test fluid is primarily a gas (air) or a liquid. A gas to gas heat exchange will be conducted in our experimental test.

The schematic of the experimental apparatus for outward corrugated tube is depicted in **Figure 4**. The system comprises a screw air compressor (the highest discharging pressure is 1.3 MPa, and the air displacement is fixed at 1.81 m³/min), two pressure-regulating valves (0.3 MPa on the hot circuit and 0.9 MPa on the cold circuit), a heater (the temperature range is 50–500°C), a test section (operating with two groups of switching valves), a measuring system (two critical Venturi flowmeters, two pressure transducers, and two temperature transducers), a data acquisition system (DAS), and a pipe system (304 stainless steel tube).

The experimental medium was air, which was compressed by the helical-lobe compressor to a pressure of 1.25 MPa. The system is made of stainless steel devices and consists of the hot circuit and cold circuit. The pressure-regulating valves adjust the air pressure to 0.3 MPa on the hot circuit and 0.9 MPa on the cold circuit with an accuracy of ±2%. The critical Venturi flowmeters control the mass flow rate in the
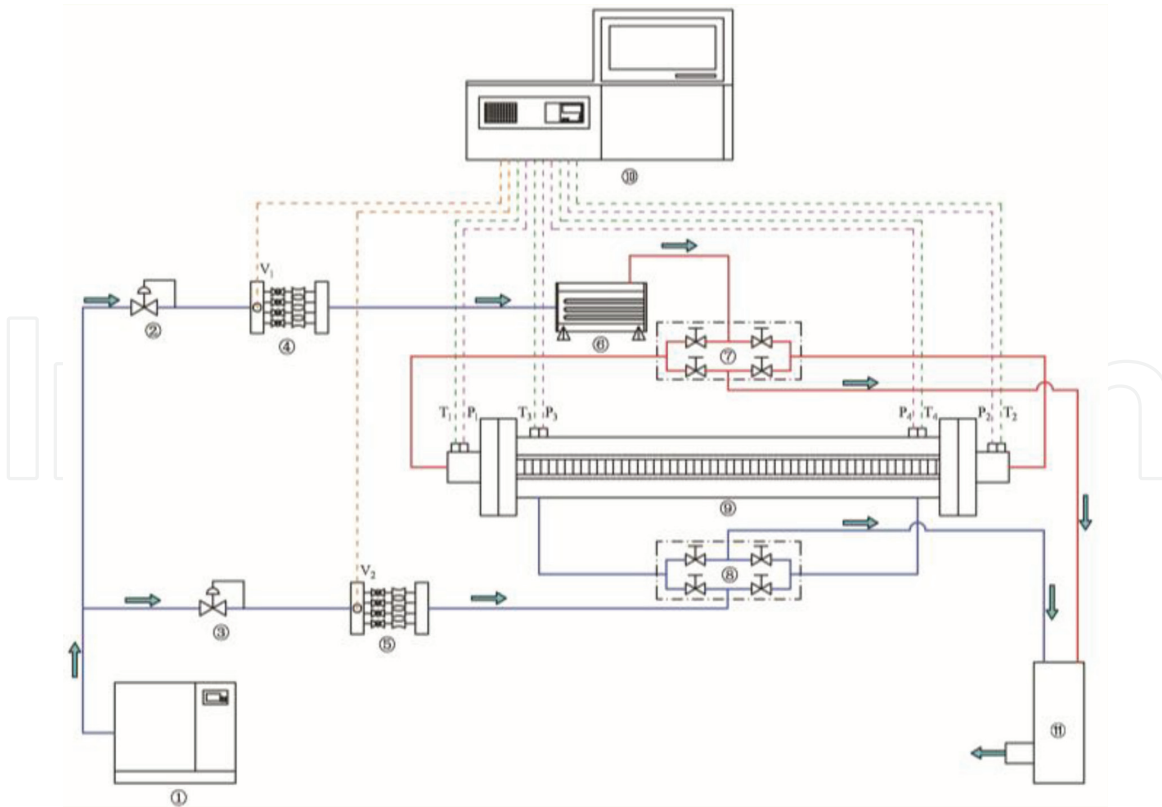
Figure 4.
System drawing of test bed. 1. Screw air compressor, 2. Pressure-regulating valve in hot circuit, 3. Pressure-regulating valve in cold circuit, 4. Critical Venturi flowmeter in hot circuit, 5. Critical flow meters in cold circuit, 6. Air heater, 7. Switching valves in hot circuit, 8. Switching valves in cold circuit, 9. Test section, 10. Data acquisition system, 11. Muffler.

hot and cold circuits. The air in the hot circuit is heated by the heater exchanger and then flows into the tube side of the test section, whereas the air in the cold circuit directly flows into the shell side. The section has a detachable structure, which enables convenient changes in various tube components. Moreover, the valve group in the vicinity of the test section makes the air flow into the tube, through either inlet of the tube side or the shell side, thus creating a uniform-current flow and a counter-current flow for each respective flow direction. Finally, the hot air and the cold air complete the heat exchange in the annular tubes of the test section, and then noise of them will be reduced through the muffler.

In the measuring system, the mass flow rates can be measured with two critical Venturi flowmeters on both circuits, with an accuracy of ±0.2%. The flow meter in the hot circuit was installed before the air heater because hot air may damage the flow meter or reduce the measurement accuracy (precision). After the heater, a temperature transducer was installed to monitor the air temperature. The DAS obtained the flow rate signal, which was transferred to a programmable logic controller (PLC) in the industrial personal computer (IPC), and the accuracy of the transformation module was ±0.05%. The pressure and temperature transducers were installed at the inlet and outlet of the section to measure the pressure and temperature of the air on both sides. All thermocouples were calibrated with an accuracy of ±0.1% of the test data. The pressure drop of the test section was measured with pressure transducers, which have an accuracy of ±0.2% and a measuring range of 0–5 kPa. The values were collected and displayed on the IPC and were automatically recorded.

The uncertainty is estimated with the method suggested by Kline and Moffat. As mentioned above, the measurement uncertainties of tube length and tube diameters are about 0.05 and 0.1%, respectively. In addition, the measurement accuracy of temperature is 0.14%, the measurement error of the differential

pressure meter is 2.06%, and the critical Venturi flowmeter has a precision of 3.11%. According to the uncertainty propagation equation, the uncertainties in the values of experimental parameters like the Reynolds number, Nusselt number, and friction factor are 3.89, 4.41, and 4.87%, respectively.

2.3 Data acquisition

The main purpose of our experimental study is to construct the relationship among the heat transfer rate q, heat transfer surface area A, heat capacity rate c of each fluid, overall heat transfer coefficient U, and fluid terminal temperatures [10]. To conduct the heat transfer analysis of an exchanger, the basic relationships that are applied for this purpose are the energy balance based on the first law of thermodynamics, as outlined in Eq. (1).

$$Q = \dot{m}\ (i_2 \text{-} i_1) \tag{1}$$

where $\dot{m}$ is the rate of mass flow, i_1 and i_2 represent the inlet and outlet enthalpies of the fluid, and Q is the heat transfer rate between hot fluid and cold fluid.

As shown in **Figure 5**, a two-fluid counterflow exchanger is considered to present variables relating to its thermal performance. Although flow arrangement may be different for different exchangers, the basic concept of modeling remains the same. The following analysis is intended to introduce important variables for heat exchanger.

If the fluids do not undergo a phase change and have constant specific heats with $di = c_p \cdot dT$, heat transfer rate released from the hot fluid (Q_h) and absorbed by the cold air (Q_c) can be expressed as

$$Q_h = \dot{m}_h C_{p,h}(T_{h_1} - T_{h_2}) \tag{2}$$

and

$$Q_c = \dot{m}_c c_{p,c}(T_{c_2} - T_{c_1}) \tag{3}$$

The subscripts h and c refer to the hot and cold fluids, and the numbers 1 and 2 designate the fluid inlet and outlet conditions, respectively.

Thus, the average value of the heat transfer rate is calculated as

$$Q_m = \frac{Q_h + Q_c}{2} \tag{4}$$

Eq. (5) reflects a convection-conduction heat transfer phenomenon in a two-fluid heat exchanger. The temperature difference between the hot and cold fluids ($\Delta T = T_h - T_c$) constantly changes along with heat exchanger. Therefore, in order to conveniently analyze the heat transfer performance of heat exchanger, it is
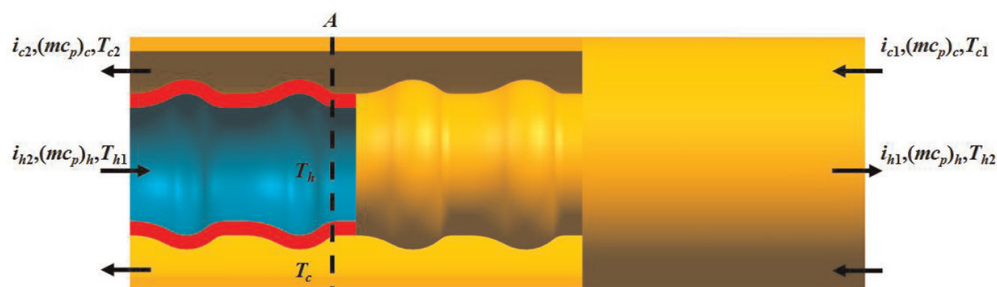

Figure 5.
The energy balance for the hot and cold fluids of a two-fluid heat exchanger.

important to establish an appropriate mean value of the temperature difference between the hot and cold fluids such that the total heat transfer rate Q between the fluids can be determined from

$$Q = UA\Delta T_{\mathrm{m}} \tag{5}$$

The heat transfer rate Q is proportional to the heat transfer area A, the average overall heat transfer coefficient based on the area U, and mean temperature difference $\Delta T_{\mathrm{max}} \Delta T_{\mathrm{m}}$ between the two fluids. This means that temperature difference is a log-mean temperature difference (for counterflow and parallel-flow exchangers).

$$\Delta T_{\mathrm{m}} = \frac{\Delta T_{\mathrm{max}} - \Delta T_{\mathrm{min}}}{\ln \frac{\Delta T_{\mathrm{max}}}{\Delta T_{\mathrm{min}}}} \tag{6}$$

ΔT_{max} and ΔT_{min}, respectively, represent the maximum and minimum one between ΔT_1 and ΔT_2.

In the experiments, the tube-wall temperature was not measured directly. The heat transfer coefficient of the tube side (h_i) is determined from:

$$\frac{1}{U} = R_t = \frac{1}{h_i} + \frac{A_i \ln (r_o/r_i)}{2\pi k L} + \frac{A_i}{A_o h_o} \tag{7}$$

where r_i and r_o are the inner radius and outer radius of the test tube, respectively. A_i and A_o are the inner and outer surface area of the tube, respectively. k is the thermal conductivity of tube material, L is the length of the heat exchange tube, and h_i and h_o are the heat transfer coefficients for inside and outside flows, respectively.

The Nusselt number can be calculated as

$$Nu = \frac{h_i \cdot D_i}{k} \tag{8}$$

where D is the characteristic diameter; the thermal conductivity k is calculated from the fluid properties at the local mean bulk fluid temperature.

The Reynolds number is based on the average flow rate of the test section.

$$Re = \frac{D \cdot u \cdot \rho}{\mu} \tag{9}$$

where μ is the dynamic viscosity of the working fluid, and u is the mean velocity. The friction factor (f) can be written as

$$f = \frac{\Delta p}{\frac{L}{D} \cdot \frac{\rho u^2}{2}} \tag{10}$$

where Δp is the pressure drop in the test section.

The performance evaluation criterion (PEC) is a dimensionless ratio, which is used for the evaluation of the overall performance of the enhanced tube and defined as follows:

$$PEC = (Nu_c/Nu_s)/\left(f_c/f_s\right)^{1/3} \tag{11}$$

When $PEC > 1$, it indicates that the enhanced tube has an advantage over the smooth tube; otherwise, the corrugated heat transfer component compares unfavorably with the smooth tube.

2.4 Heat and mass transfer performance

For the engineering applications and to design exchangers, the prediction of heat and mass transfer performance is important. We presented experimental data on the Nusselt numbers for turbulent regimes. In our experimental study, the hot fluid is at the tube side, and the cold fluid is at the shell side.

The heat transfer and resistance performance of corrugated tube are compared to smooth tube, aiming to reflect the superior of the corrugated tube. Ratio of Nu in the corrugated tube to that in the smooth tube (Nu_c/Nu_s) and ratio of f in the corrugated tube to that in the smooth tube (f_c/f_s) are adopted to indicate the enhancement degree of heat transfer and flow resistance performance.

Figure 6 shows the effect of Re_c (Re of the cold fluid) on Nu_c/Nu_s, f_c/f_s, and PEC, along with the changing Re_h (Re of the hot fluid). The figure exhibits that with the increase of Re, Nu_c/Nu_s, f_c/f_s, and PEC decline. The decreasing rate of Nu_c/Nu_s and PEC is almost linear, but f_c/f_s is decelerated.
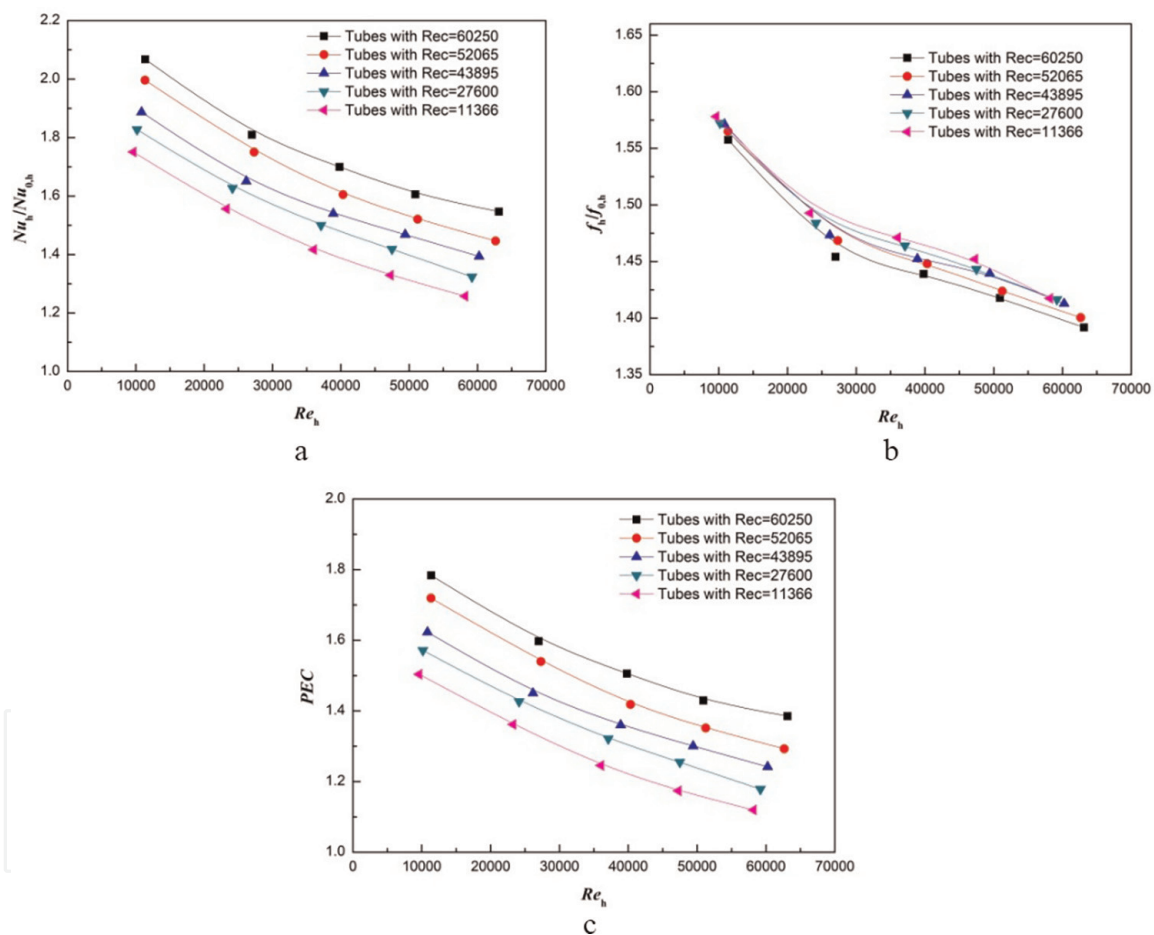

Figure 6.
Flow and mass transfer performance. (a) Nuc/Nus; (b) f/fs; (c) PEC.

3. Heat and mass transfer at outward convex corrugated tube heat exchangers

3.1 Numerical methods

3.1.1 Physical model and meshing system

The first task to accomplish in a numerical simulation is the definition of the geometry followed by the mesh generation. The geometry of the design needs to be

created from the initial design. Any modeling software can be used for modeling and shifted to other simulation software for analysis purpose.

Figure 7 shows a schematic view of the structural parameters for corrugated tube investigated in this chapter, which include inner diameter (D), tube length (L), corrugation height (H), corrugation pitch (P), corrugation crest radius (R), and corrugation trough radius (r). Since the investigated corrugated tubes are used in tube-shell type heat exchanger, the flow region inside of tube is named "tube side" and out of tube is named "shell side."

Mesh generation is the process of subdividing a region to be modeled into a set of small control volumes. In general, a control volume model is defined by a mesh network, which is made up of the geometric arrangement of control volumes and nodes. Nodes represent points at which features such as displacements are calculated. Control volumes are bounded by set of nodes and also defined by the number of mesh. One or more values of dependent flow variable (e.g. velocity, pressure, temperature, etc.) will be contained in each control volume. Usually, these represent some type of locally averaged values. Numerical algorithms representing approximation to the conservation law of mass, momentum, and energy are then used to compute these variables in each control volume.

Mesh generation is often considered as the most important and most time consuming part of CFD simulation [13]. The quality of the mesh plays a direct role on the quality of the analysis, regardless of the flow solver used. In this work, a 3D non-uniform mesh system of hexahedral elements was established via the professional mesh generation software ICEM to accurately control the size and number of cells in the domain, as illustrated in **Figure 8**. The near-wall vicinity should be present
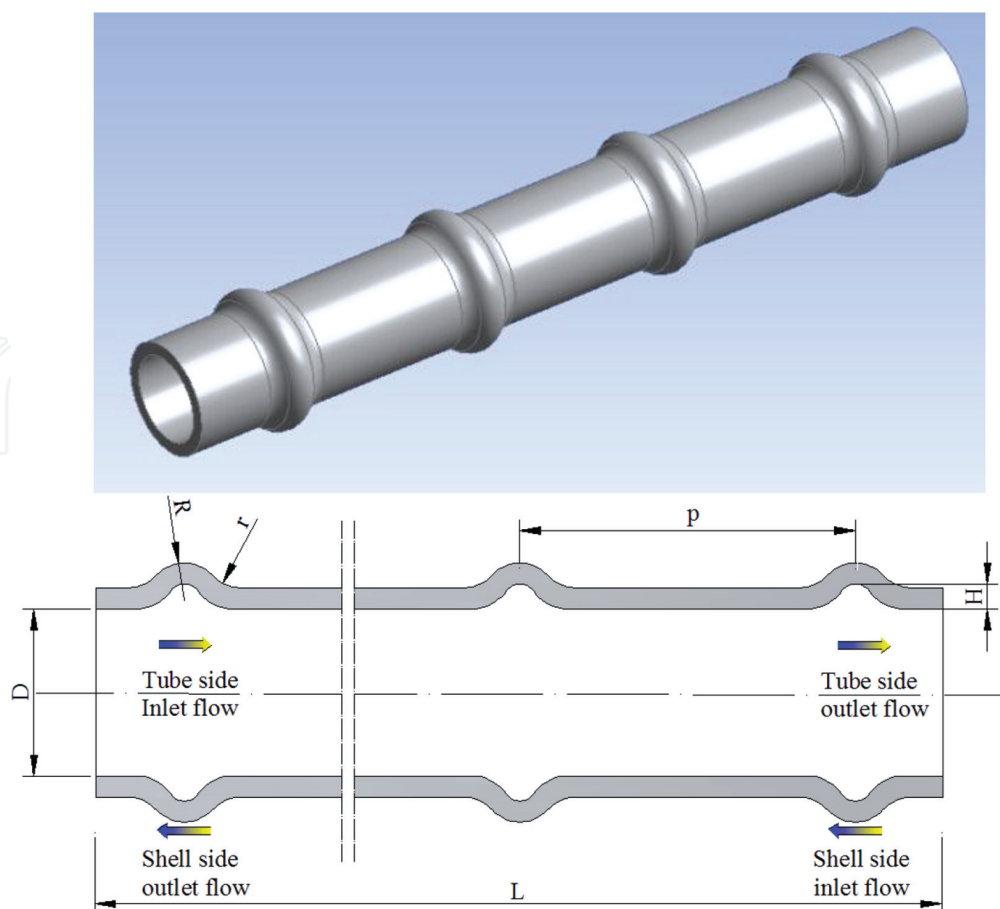

Figure 7.
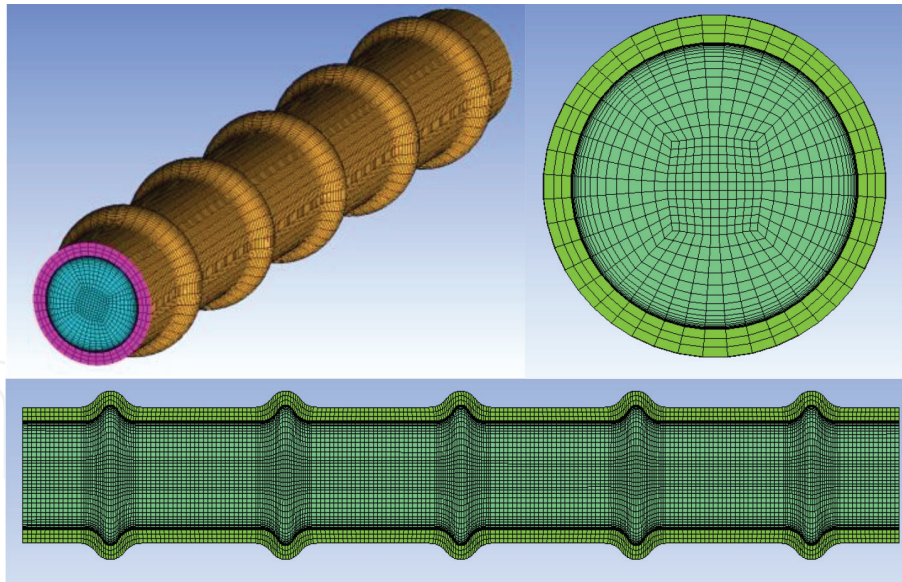*Structure parameters of outward convex corrugated tube.*

Figure 8.
Schematic diagram of meshing system for the simulated corrugated tube.

drastic velocity and temperature gradients, so a high density of gradient elements was applied in this region. Nevertheless, the remaining domain was modeled with relatively sparse elements. The first layer of thickness should satisfy $y^+ \approx 1$.

3.1.2 Mathematical model

Mathematical model should be constructed to numerically describe flow and heat transfer of corrugated tube. The Navier-Stokes equations generally are adopted to describe the laminar and turbulent flows, which could be solved by various kinds of simulation model including DNS, LES, and RANS. The direct numerical simulation (DNS) can solve accurately the turbulent fluctuation, but these models require huge computing power, which is many orders of magnitude higher than other models. Reynolds-averaged Navier-Stokes (RANS) is a high efficient model that can be used to approximate turbulence by time-averaged turbulent fluctuation, but the accuracy of the models is much less than DNS. The accuracy and efficient of LES are between the DNS and RANS.

The k-ε (k-epsilon) model is one of the most prominent RANS models, which has been implemented in most CFD codes and is considered the most common industry model. The stability and robustness of the models have a well-established regime of predictive capability, satisfying general purpose simulation by offering a comparative good accuracy. In our research work for outward convex corrugated tube, we use standard k-ε model for numerical simulation research.

The governing equations in a RANS (Reynolds Averaged Navier-Stokes) manner are given below.

Continuity equation:

$$\frac{\partial(\rho u_i)}{\partial x_i} = 0 \tag{12}$$

Momentum equation:

$$\frac{\partial}{\partial x_j}\left(\rho u_i u_j\right) = -\frac{\partial P}{\partial x_i} + \frac{\partial}{\partial x_j}\left[\mu\left(\frac{\partial u_i}{\partial x_j} + \frac{\partial u_j}{\partial x_i} - \frac{2}{3}\delta_{ij}\frac{\partial u_k}{\partial x_k}\right)\right] + \frac{\partial}{\partial x_j}\left(-\rho\overline{u_i' u_j'}\right) \tag{13}$$

Energy equation:

$$\frac{\partial}{\partial x_i}[u_i(\rho E + P)] = \frac{\partial}{\partial x_j}\left[\left(\lambda + \frac{c_p \mu_t}{Pr_t}\right)\frac{\partial T}{\partial x_j} + \mu_{\text{eff}} u_i\left(\frac{\partial u_i}{\partial x_j} + \frac{\partial u_j}{\partial x_i} - \frac{2}{3}\delta_{ij}\frac{\partial u_k}{\partial x_k}\right)\right] \quad (14)$$

The standard k-ε model is adopted here to close governing equations:

$$\frac{\partial}{\partial x_i}(\rho k u_i) = \frac{\partial}{\partial x_j}\left[\left(\mu + \frac{\mu_t}{\sigma_k}\right)\frac{\partial k}{\partial x_j}\right] + G_k - \rho\varepsilon \quad (15)$$

$$\frac{\partial}{\partial x_i}(\rho\varepsilon u_i) = \frac{\partial}{\partial x_j}\left[\left(\mu + \frac{\mu_t}{\sigma_\varepsilon}\right)\frac{\partial\varepsilon}{\partial x_j}\right] + C_{1\varepsilon}\frac{\varepsilon}{k}(G_k) - C_{2\varepsilon}\rho\frac{\varepsilon^2}{k} \quad (16)$$

where μ_t is the turbulent or eddy viscosity, and G_k represents the generation of turbulent kinetic energy due to the mean velocity gradients. The model constants $C_{1\varepsilon}$, $C_{2\varepsilon}$, C_μ, σ_k, and σ_ε are chosen for the default values 1.44, 1.92, 0.09, 1.0, and 1.30, respectively.

3.1.3 Boundary and initial condition

The next step in preprocessing is setting up the boundary conditions. Boundary conditions refer to the conditions that the solution of the equations should satisfy at the boundary of the moving fluid. Boundary condition will be different for each type of problem. In our research work, the initial and boundary conditions of the outward convex corrugated tube heat exchangers are shown as follows:

1. The inlet conditions at the shell side are as follows: velocity inlet $U = U_{\text{in}}$, $T_{\text{in}} = 563.15$ K, and the inlet turbulence specifications are a turbulence intensity of $I = 5\%$ and hydraulic diameter $D = 20$ mm.

2. The outlet conditions at the shell side are as follows: pressure outlet, $P_o = 7$ MPa, and the outlet turbulence specifications are a turbulence intensity of $I = 5\%$ and a viscosity ratio $\mu_t/\mu_{\text{lam}} = 5\%$.

3. The wall conditions are as follows: the outer wall temperature boundary condition is constant, $T_w = 700$ K, and the inner wall-coupled boundary condition was set as a no-slip boundary, $u = v = w = 0$, $T = T_w$, and $q = q_w$.

3.1.4 Numerical procedure

The final step in preprocessing is setting up the numerical procedure, which includes solver, discretization, and convergence criterion. In our work, the governing equations are discretized by the finite volume method and solved by the steady-state implicit format. The SIMPLE algorithm is used to couple the velocity and pressure fields. The second-order upwind scheme is applied herein. The convergence criterion for energy is set to be 10^{-7} relative error and 10^{-4} relative error for other variables.

3.2 Heat and mass transfer in tube and shell side of corrugated tube

The variable distribution exhibits the opposite similar tendency at the shell side compared with that at the tube side. In this chapter, we mainly analyze the distribution of velocity, temperature, and turbulence kinetic energy.

3.2.1 Flow structure

Figure 9(a) shows the velocity vector distribution in the tube side of outward convex corrugation tube. As shown from this figure, when fluid flow starts to cross the corrugation section bended from the straight segment, the flow boundary layer separates into two parts: one is the wall boundary layer developed at the near wall region; the other is shear layer associated with an inflection point of large velocity gradient developed away from the wall, which moves away from the surface at the separation point and forms a free shear layer. When the fluid flows through the upstream of the corrugation, the flow velocity decreases and the pressure increases due to the narrowing of the flow cross section. The fluid layer near the wall is gradually difficult to overcome the rising pressure due to the small amount of momentum, resulting in a reflow of the original flow direction. The recirculating zone between the separating streamline and the free boundary streamline is generated at the upstream of the corrugation.

Figure 9(b) indicates the velocity vector distribution in the shell side of outward convex corrugation tube. As shown in this figure, the upstream side boundary of the corrugation is influenced by the accelerating outer-flow, that is, a favorable gradient. As the boundary layer thickens, instabilities occur when the near-wall fluid begins to decelerate as shown in **Figure 7**. The flow separates at the downgrade of the corrugation crest, which is associated with an inflection point of the large velocity gradient developed away the wall.

3.2.2 Temperature distribution

Figure 10(a) shows the temperature distribution in the tube side of outward convex corrugation tube. As shown in **Figure 8**, the wall velocity boundary layer becomes thicker at the upstream side of the corrugation accompany gradually, while the temperature boundary layer gets thicker along the flow direction, due to the eddy generating. Then it goes into thinner at the downstream side of the corrugation with the velocity boundary layer getting thinner, due to the scouring action of the fluid.

Figure 10(b) shows the temperature distribution in the tube side of outward convex corrugation tube. As shown in **Figure 9**, the wall velocity boundary layer becomes thicker at the downstream side of the corrugation accompany gradually, while the temperature boundary layer gets thicker along the flow direction, due to the eddy generating. Then, it goes into thinner at the upstream side of the corrugation with the velocity boundary layer getting thinner, due to the scouring action of the fluid. The thinnest temperature boundary layer occurs at the corrugation crest.
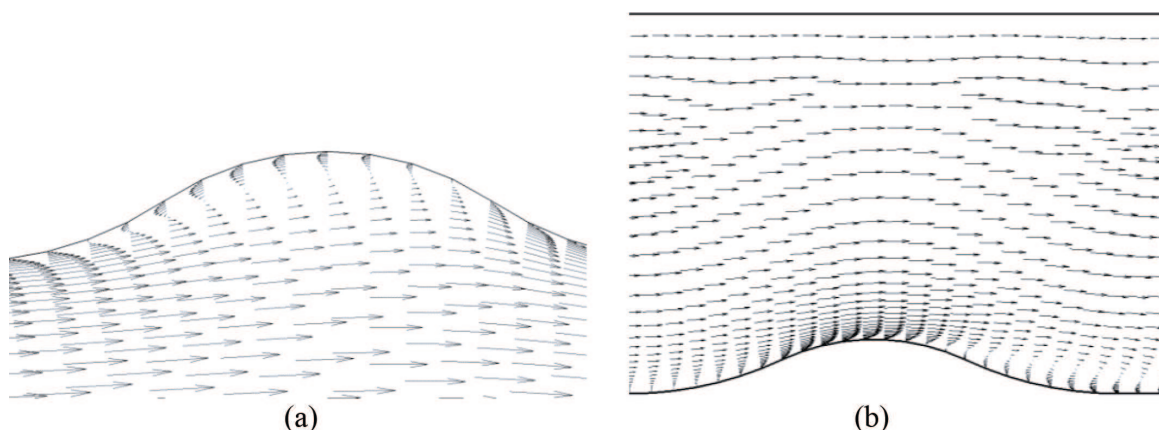

(a)   (b)

Figure 9.
Velocity vector distribution at tube side and at shell side. (a) tube side; (b) shell side.

Figure 10.
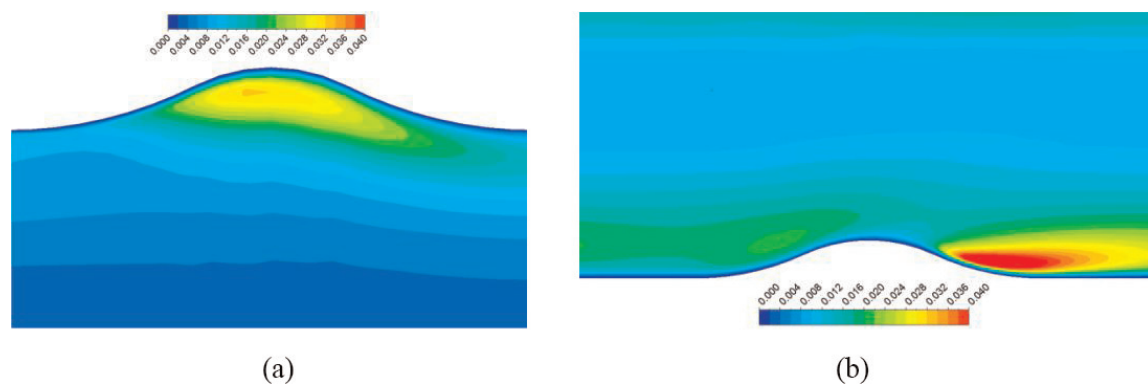*Temperature distribution at tube side and at shell side. (a) tube side; (b) shell side.*

Figure 11.
TKE distribution at tube side and at shell side. (a) tube side; (b) shell side.

3.2.3 Turbulence kinetic energy

Turbulence kinetic energy (TKE) is one of the most important variables in boundary layer since it is a measure of the turbulence intensity, which is tightly related to the velocity profile. **Figure 11(a)** shows the turbulence kinetic energy distribution in the tube side of outward convex corrugation tube. As shown in this figure, the magnitude of the TKE gradient increases past upstream side section of corrugation with a noticed reduction after the flow reattaches as it enters downstream side section of corrugation. The location of the maximum turbulence kinetic energy extends over most of the corrugation, before descending when passing the downstream section of the wave trough.

Figure 11(b) shows the turbulence kinetic energy distribution in the tube side of outward convex corrugation tube. As shown in this figure, the magnitude of the high TKE extends fairly constant past most of the corrugation with a noticed reduction after the flow reattaches. The location of the high TKE extends over most of corrugation at a height, which roughly equals to the maximum corrugation height, before subsiding toward the corrugation trough.

4. Heat and mass transfer enhancement of outward convex corrugated tube heat exchangers

4.1 Enhancement methods

Heat transfer enhancement methods are classified into three classifications: active, passive, and compound. The active methods include electrostatic and

magnetic fields, induced pulsation, mechanical aid, vibration, and jet impingement. These methods require external activating power to enhance the heat transfer [3–6]. Passive methods modify the geometrical structure to expand the effective surface area to disturb the actual boundary layer. Compound methods combine the two heat transfer augmentation methods to increase heat transfer performance. In the above-mentioned methods, passive methods have attracted significant attention from researchers and engineers since they are user-friendly and affordable. Extensive research has been devoted to develop highly efficient heat transfer components to better understand the physical mechanisms and optimal parameters of passive heat transfer augmentation methods.

The heat transfer enhancement mechanism in the corrugated tube is described as follows. The periodically corrugated structure on the tube wall arouses periodic alteration of velocity gradient, leading to adverse and favorable pressure gradient locally. The recurrent alternation of axial pressure gradient induces the secondary disturbance, and then the produced intensive eddy destroys the flow boundary layer. The eddy also increases the turbulence intensity of the flow. The disturbance caused by corrugated structures thus increases the heat transfer coefficient drastically.

4.2 Tube side enhancement

Figure 12 shows the effect of Re on Nu_c with various p/D and H/D. The Nu_c tends to increase linearly with the increasing Re with a fixed structure of the corrugated tube. This behavior occurs because the increases of flow velocity break wall thermal boundary layer and could obtain higher convective heat transfer coefficient. Moreover, with the decreasing p/D and increasing H/D, the values of the Nu_c increase.

In order to compare the performance between corrugated tube and smooth tube, the ratio of Nu in the corrugated tube to that in the smooth tube (Nu_c/Nu_s) is adopted to indicate the relative grow rate of heat transfer performance. **Figure 13** shows the effect of Re on Nu_c/Nu_s with various p/D and H/D, and the figure exhibits that with the increase of Re, Nu_c/Nu_s declines deceleratedly. Moreover, the Nu_c/Nu_s increases with the decreasing p/D and increasing H/D.

4.3 Shell side enhancement

Figure 14 shows the effect of Re on Nu_c with various p/D and H/D in the shell side. Compared with **Figure 12**, the changing tendency of Nu_c along with Re, p/D,
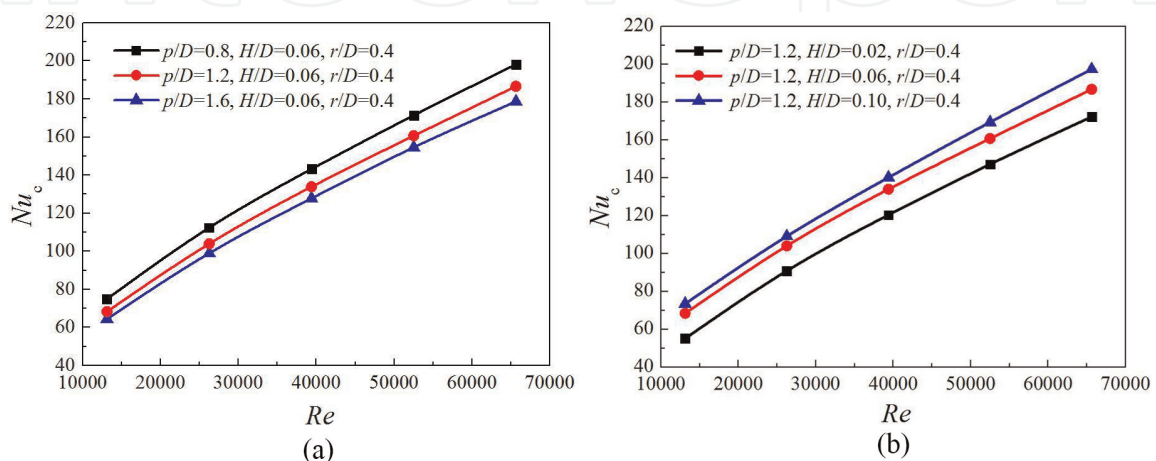
Figure 12.
Effect of Re on Nu with various p/D and H/D in the tube side. (a) various p/D (b) various H/D.
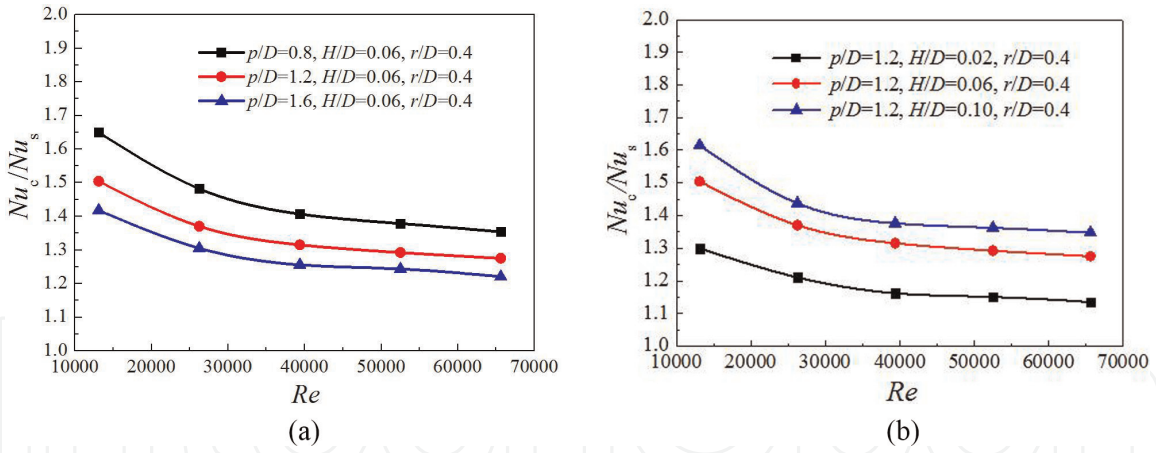
Figure 13.
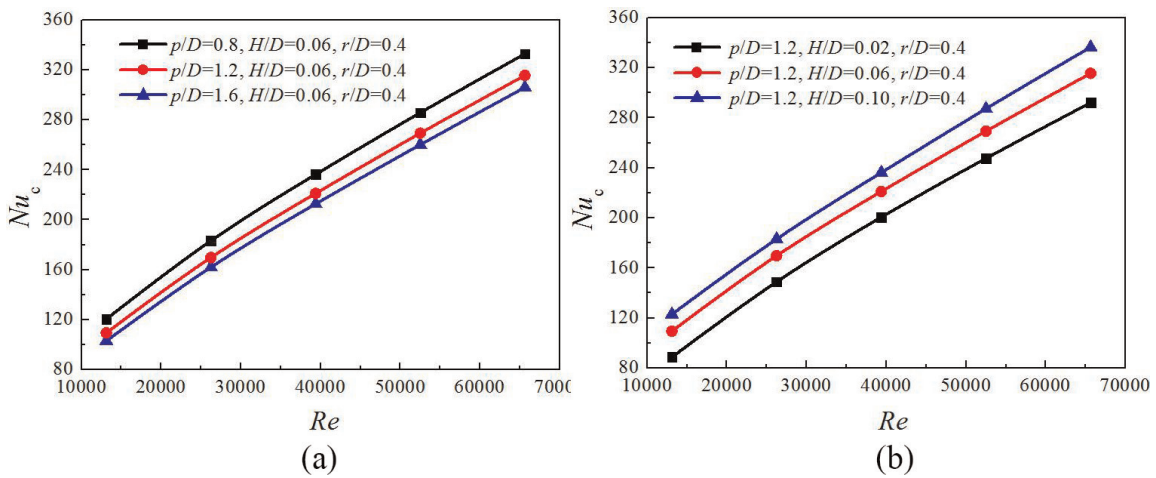*Effect of Re on Nu_c/Nu_s with various p/D and H/D in the tube side. (a) various p/D (b) various H/D.*

Figure 14.
Effect of Re on Nu with various p/D and H/D in the shell side. (a) various p/D (b) various H/D.

and *H/D* is consistent, but the Nu_c in the shell side is obviously higher than in the tube side.

Figure 15 shows the effect of *Re* on Nu_c/Nu_s with various *p/D* and *H/D* in the shell side. It can be found when compared with **Figure 13**, the changing tendency of Nu_c/Nu_s along with *Re*, *p/D,* and *H/D* is also consistent, but the Nu_c/Nu_s in the shell side is obviously higher than in the tube side.
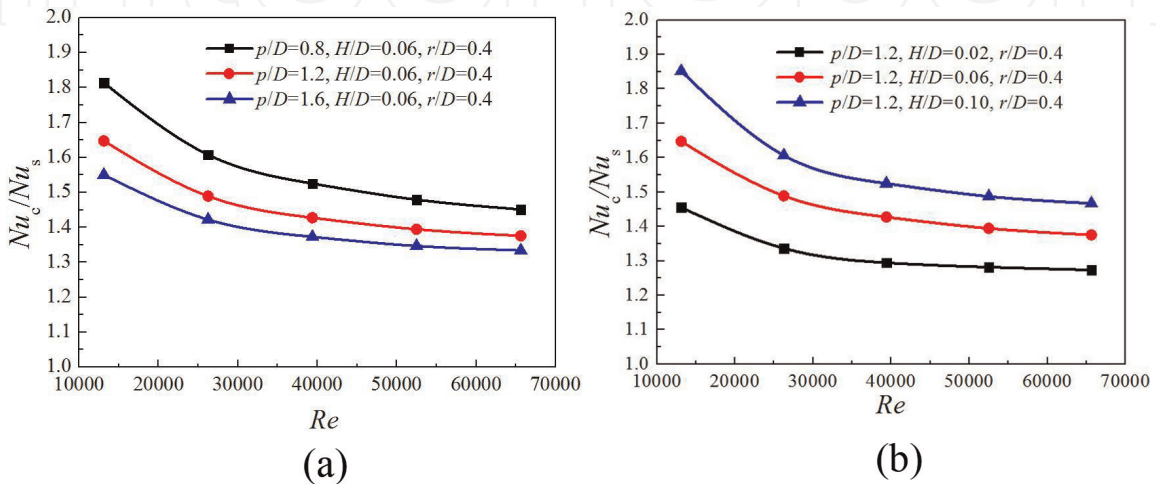

Figure 15.
Effect of Re on Nu with various p/D and H/D in the shell side. (a) various p/D (b) various H/D.
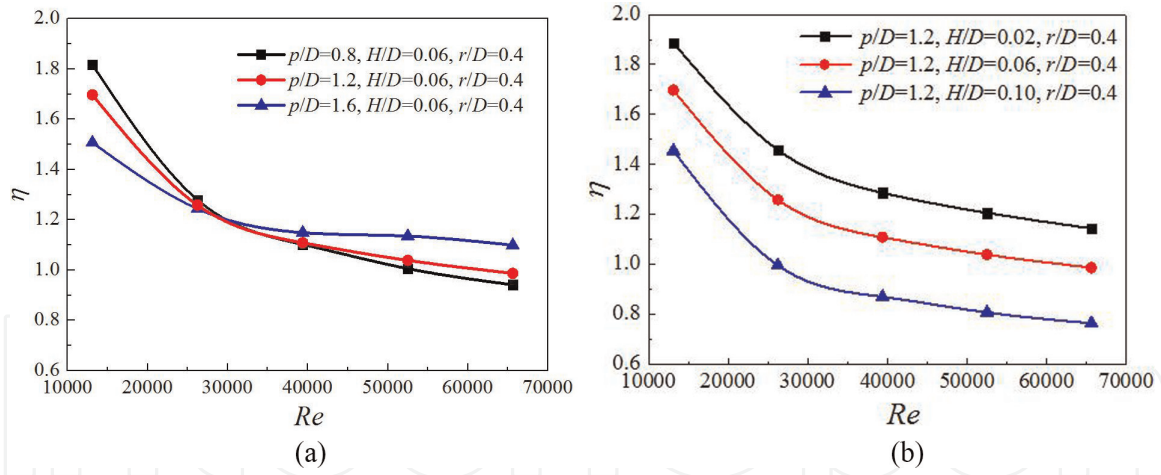
Figure 16.
Effect of Re on η with various p/D and H/D in the tube side. (a) various p/D (b) various H/D.

4.4 Overall enhancement

Generally, heat transfer enhancement accompanies with a penalty of flow resistance when a heat transfer enhancement component (corrugated tube in this paper) is utilized in a heat exchanger compared to the smooth tube. Therefore, an assessment criterion needs to be constructed to evaluate the overall heat transfer performance for the investigated corrugated tube. The function of overall heat transfer performance is adopted as follows:

$$\eta = (Nu_c/Nu_s)/(f_c/f_s)^{1/3} \tag{17}$$

Figure 16 indicates the effect of *Re* on overall heat transfer performance (*η*) with various *p/D* and *H/D* in the tube side of outward convex corrugated tube. The figure displays that with the increase of *Re*, *η* declines deceleratedly. This is because the Nu_c/Nu_s gradually decreases along with increasing *Re*. In addition, with the increase of *p/D*, *η* decreases when *Re* < 30,000, but increases when *Re* > 30,000. This can be explained from the fact that decreasing extent of Nu_c/Nu_s is larger than that of f_c/f_s with increase in *p/D* when *Re* < 30,000, but lower when *Re* > 30,000. Moreover, the *η* decreases obviously with the increasing
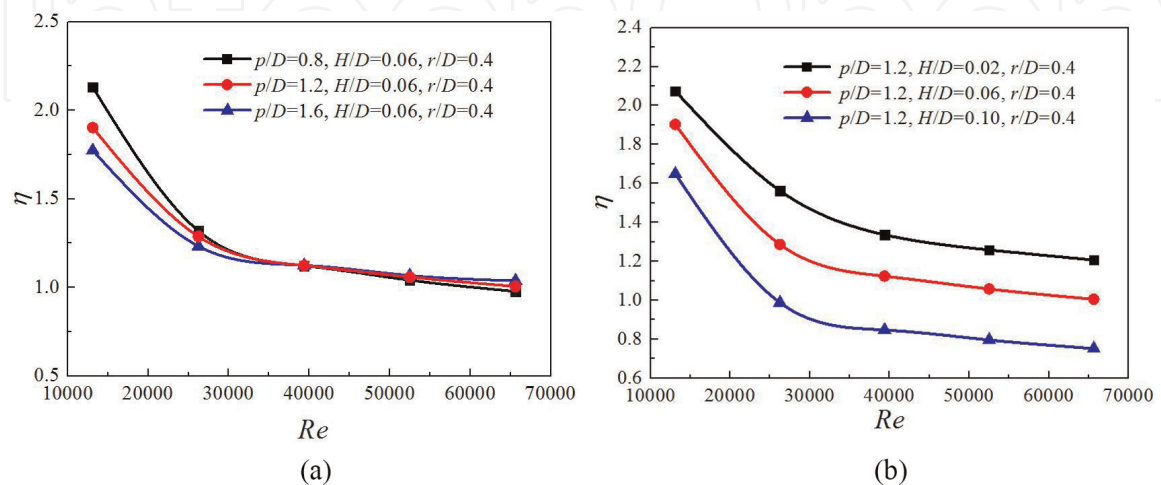

Figure 17.
Effect of Re on η with various p/D and H/D in the shell side. (a) various p/D (b) various H/D.

H/D, and the decreasing extent from $H/D = 0.02$ to $H/D = 0.06$ is more obvious than that from $H/D = 0.06$ to $H/D = 0.10$. This variation is quite intuitive because of the fact that increasing extent of Nu_c/Nu_s is larger than that of f_c/f_s along with increasing H/D.

It can be observed from **Figure 17** that the changing trend of η with various p/D and H/D in the shell side is almost the same from the tube side. However, the values of η in the shell side are larger than in the tube side. Therefore, the overall heat transfer enhancement in the shell side is superior to the tube side.

5. Optimization of outward convex corrugated tube heat exchangers

5.1 Optimization methods

Response surface methodology (RSM) is composed of a series of statistical and mathematical method for analyzing empirical results, which can construct connection between effect factors and objective functions. The sensitivity of each effect factor and the interactions between two factors can also be analyzed to the objective functions. Recently, RSM has been extensively used to study on the optimal design of heat exchangers, which is able to efficiently and accurately provide the design consideration for heat exchangers [7–9].

RSM constructs the relationship between objective functions and design variables using a series of statistical and mathematical methodology. The function expression of the relationship could be written as follows:

$$G = f(X_1, X_2, ..., X_k) + \varepsilon \tag{18}$$

where G represents the objective functions and X_1, X_2, ..., X_k stand for design variables, f represents an approximate function, and ε is the residual error between the real value and the approximate value. The approximate functions are described as a quadratic polynomial, aiming to reflect the nonlinear characteristic between objective functions and design variables. In this study, the quadratic polynomial function, including the linear, square, and interaction terms, can be expressed as follows:

$$G = b_0 + \sum_{I=1}^{N}(b_I X_I) + \sum_{I=1}^{N-1}\sum_{J=I+1}^{N}(b_{I,J} X_I X_J) + \sum_{I=1}^{N}(b_{I,I} X_I^2) + \varepsilon \tag{19}$$

where b_I represents the linear effect of design variable X_I, $b_{I,I}$ represents the quadratic effect of X_I, and $b_{I,J}$ represents the linear-linear interactions between X_I and X_J.

5.1.1 Optimization procedure

In our present work, we adopted the flow chart of optimization procedure as shown in **Figure 18**. Three objective functions including heat transfer, pressure drop, and overall heat transfer performance in a heat exchanger tube are selected for optimization. In this simulation plan, a most popular design method called the design of experiment (DOE) and central composite design (CCD) is applied. As shown in **Figure 19**, points including factorial points and center points augmented
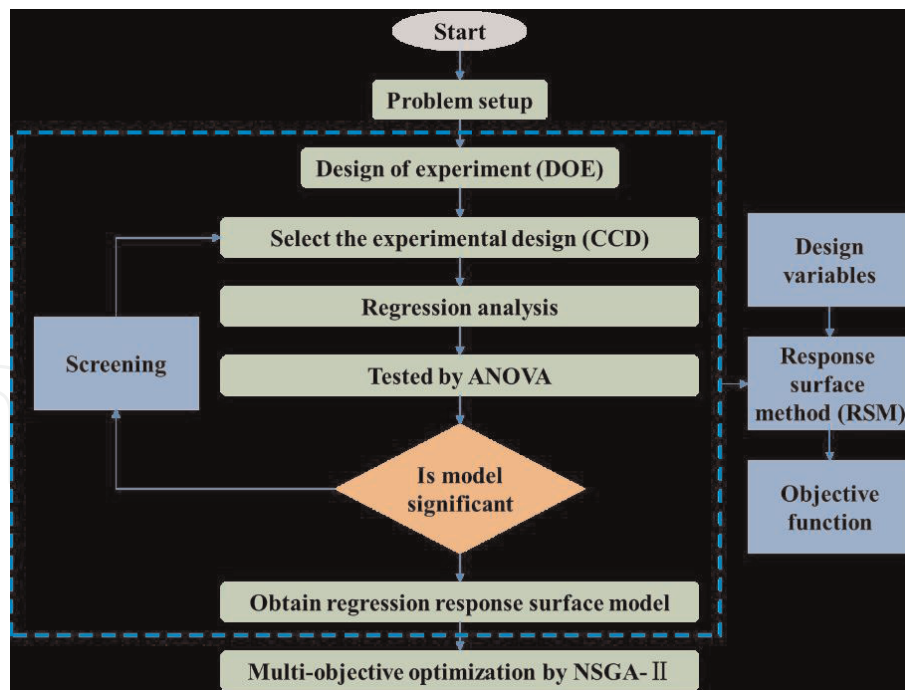
Figure 18.
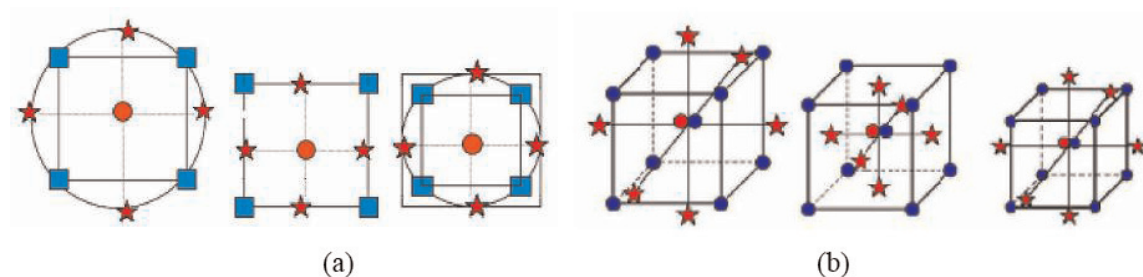*Flow chart of optimization procedure.*

Figure 19.
CCD model. (a) Two factors. (b) Three factors.

by axial points are set in CCD. The numerical results for DOE runs are utilized in reflecting the behavior of responses with geometrical and flow parameters.

5.1.2 NSGA-II algorithm

Nondominated sorting genetic algorithm II (NSGA-II) combined with the multi-objective optimization is adopted in this study. The advantages of NSGA-II are a uniformly distributed Pareto-optimal front, which can suitably detect Pareto-optimal front for multi-objective problems, decrease time consuming, and present solutions with a single run.

Figure 20 shows the NSGA-II flowchart. As specified in **Figure 18**, the RSM has been employed to determine the fitness functions in the optimization algorithm. As well, cross over and mutation contained in genetic operators are used in order to generate a new population. Finally, the optimization process is wrapped up with condition of repetitions number.

This algorithm uses two functions including nondominated sorting function and crowding distance function, respectively. This subprogram takes population members as input, ranks them, and puts them into fronts in proportion to their ranks. Crowding distance function has been designed to avoid the accumulation of
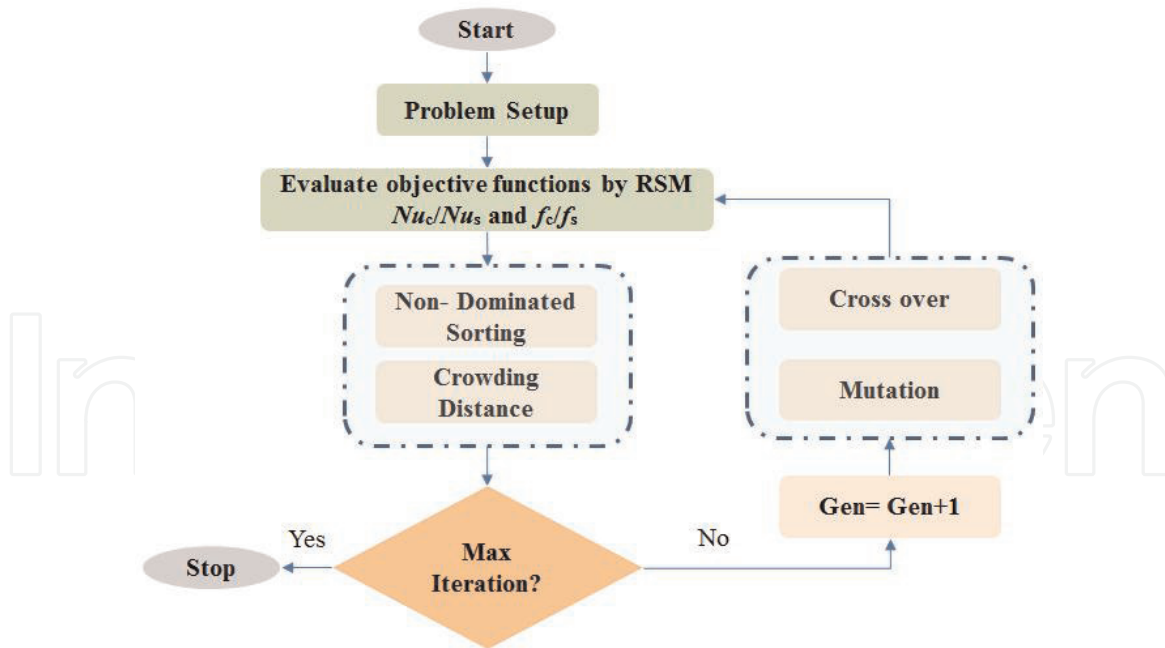
Figure 20.
NSGA-II flowchart.

population members in a limited distance. On the other hand, there are no blank intervals in the domain by using crowding distance function. The function is applied for comparison between members of a front that has equal ranks. Compared to the previous and the next member and also the first and the last member of the population, the normalization Euclidean distance of each solution of the front is for each reference point. Normalization is applied to avoid the problem that the objectives are in the different scale.

5.2 Analysis of variance

ANOVA is one statistical analysis method used to evaluate the fitness of regression models, perform significance testing, and construct simplified regression models between design factors and objective functions. **Tables 1** and **2** are ANOVA for Nu_c and f_c. According to the values of R^2, the fitting degree of the RSM is estimated. The F value and P value indicate the influencing significances of the model terms, judging the significant degree of each model term for the global sensitivity analysis. If the model term is the most significant, the corresponding P value is minimum, and F value is maximum. Generally, the terms having a P value >0.05 are considered insignificant and are removed from the models.

5.3 Regression model of responses

The regression response surface models are described in quadratic polynomial form. Coefficients in the models are determined based on a series of statistical and mathematical methods. The models evaluate the objective functions G including Nu_c/Nu_s, f_c/f_s, and η, which are expressed as:

$$G = b_0 + b_1 \cdot Re + b_2 \cdot Y + b_3 \cdot CR + b_{1,2} \cdot Re \cdot Y + b_{1,3} \cdot Re \cdot CR$$
$$+ b_{2,3} \cdot Y \cdot CR + b_{1,1} \cdot Re^2 + b_{2,2} \cdot Y^2 + b_{3,3} \cdot CR^2$$

(20)

Source	DF	Seq SS	Adj SS	Adj MS	F	P
Regression	14	112756	112756	8054	1893.32	0.000
Linear	4	111873	111873	27968	6574.69	0.000
p/D	1	2398	2398	2398	563.65	0.000
H/D	1	8140	8140	8140	1913.54	0.000
r/D	1	186	186	186	43.80	0.000
Re	1	101149	101149	101149	23777.79	0.000
Square	4	63	63	16	3.73	0.042
$(p/D)\cdot(p/D)$	1	1	28	28	6.65	0.028
$(H/D)\cdot(H/D)$	1	37	17	17	4.03	0.073
$(r/D)\cdot(r/D)$	1	0	3	3	0.61	0.452
$Re\cdot Re$	1	25	25	25	5.94	0.035
Interaction	6	820	820	137	32.13	0.000
$(p/D)\cdot(H/D)$	1	585	585	585	137.46	0.000
$(p/D)\cdot(r/D)$	1	9	9	9	2.00	0.187
$(p/D)\cdot Re$	1	33	33	33	7.76	0.019
$(H/D)\cdot(r/D)$	1	11	11	11	2.64	0.135
$(H/D)\cdot Re$	1	178	178	178	41.90	0.000
$(r/D)\cdot Re$	1	4	4	4	1.01	0.339
Residual Error	10	43	43	4		
Total	24	112799				

Standard deviation $= 2.06$
Predicted residual error of sum of squares (PRESS) $= 268.69$
R^2 (Adequate) $= 99.96\%$ R^2 (Predicted) $= 99.76\%$ R^2 (Adjusted) $= 99.91\%$

Table 1.
Analysis of variable (ANOVA) for Nu_c.

In our optimum work, the regression response surface models for evaluating Nu_c and f_c are expressed as:

$$Nu_c = 64.89 - 51.44p/D + 1026.68H/D - 34.95r/D + 0.0046Re - 377.83p/D \cdot H/D$$
$$- 1.82(\text{E} - 04)p/D \cdot Re + 0.0042H/D \cdot Re + 20.83(p/D)^2 - 8.12(\text{E} - 09)Re^2$$

$$(21)$$

$$f_c = 0.077 - 0.05p/D + 1.21H/D - 0.037r/D - 7.76(\text{E} - 07)Re - 0.57p/D \cdot H/D$$
$$+ 0.012p/D \cdot r/D - 0.38H/D \cdot r/D - 4.41\,(\text{E} - 06)H/D \cdot Re$$

$$(22)$$

5.4 Response surface analysis

We applied 2D response surface contour plots to describe the regression response surface model, in order to display the interaction influence of each pair of design variables on the required responses. From the 2D response surface contour plots, the regulation of objective functions with changing design variables can be clearly observed, distinguished by contour plot color. **Figures 21** and **22** show the 2D surface plots of the combined effects for the standard deviation of Nu_c and f_c. It

Source	DF	Seq SS	Adj SS	Adj MS	F	P
Regression	14	0.019961	0.019961	0.001426	157.04	0.000
Linear	4	0.017620	0.017620	0.004405	485.16	0.000
p/D	1	0.002109	0.002109	0.002109	232.28	0.000
H/D	1	0.014332	0.014332	0.014332	1578.59	0.000
r/D	1	0.000275	0.000275	0.000275	30.27	0.000
Re	1	0.000904	0.000904	0.000904	99.51	0.000
Square	4	0.000599	0.000599	0.000150	16.51	0.000
$(p/D) \cdot (p/D)$	1	0.000380	0.000022	0.000022	2.40	0.152
$(H/D) \cdot (H/D)$	1	0.000209	0.000131	0.000131	14.47	0.003
$(r/D) \cdot (r/D)$	1	0.000004	0.000002	0.000002	0.18	0.681
$Re \cdot Re$	1	0.000006	0.000006	0.000006	0.69	0.426
Interaction	6	0.001742	0.001742	0.000290	31.97	0.000
$(p/D) \cdot (H/D)$	1	0.001342	0.001342	0.001342	147.76	0.000
$(p/D) \cdot (r/D)$	1	0.000014	0.000014	0.000014	1.57	0.239
$(p/D) \cdot Re$	1	0.000034	0.000034	0.000034	3.80	0.080
$(H/D) \cdot (r/D)$	1	0.000147	0.000147	0.000147	16.18	0.002
$(H/D) \cdot Re$	1	0.000193	0.000193	0.000193	21.28	0.001
$(r/D) \cdot Re$	1	0.000011	0.000011	0.000011	1.25	0.290
Residual Error	10	0.000091	0.000091	0.000009		
Total	24	0.020052				

Standard deviation = 0.003
Predicted residual error of sum of squares (PRESS) = 0.00057
R^2 (Adequate) = 99.55% R^2 (Predicted) = 97.16% R^2 (Adjusted) = 98.91%

Table 2.
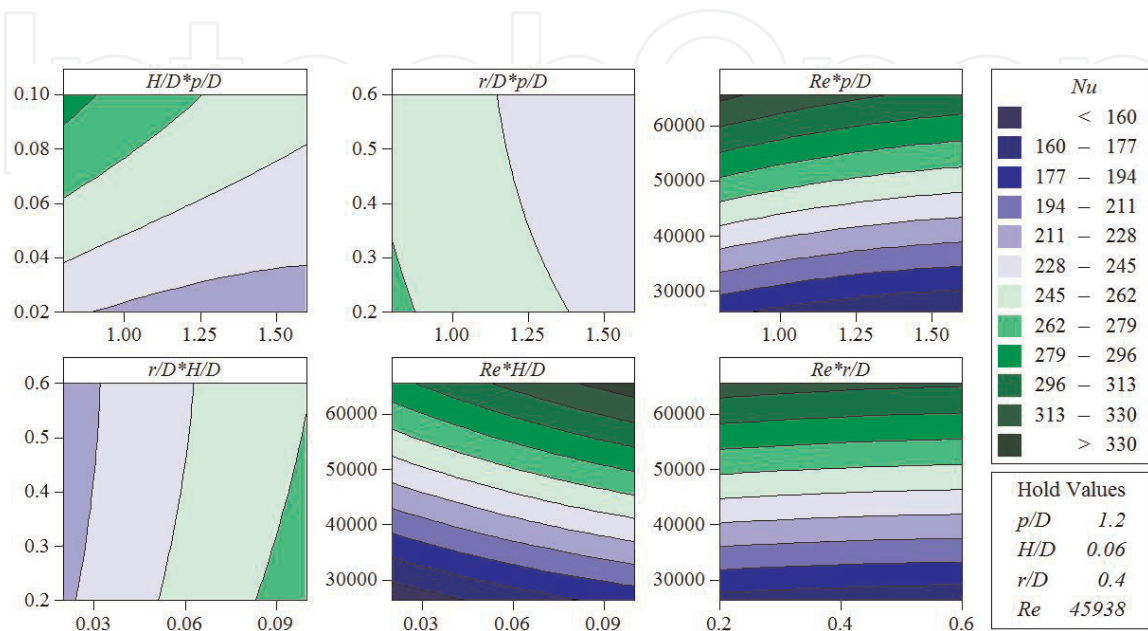*Analysis of variable (ANOVA) for f_c.*

Figure 21.
Response surfaces contour plots of combined effects for Nu_c.
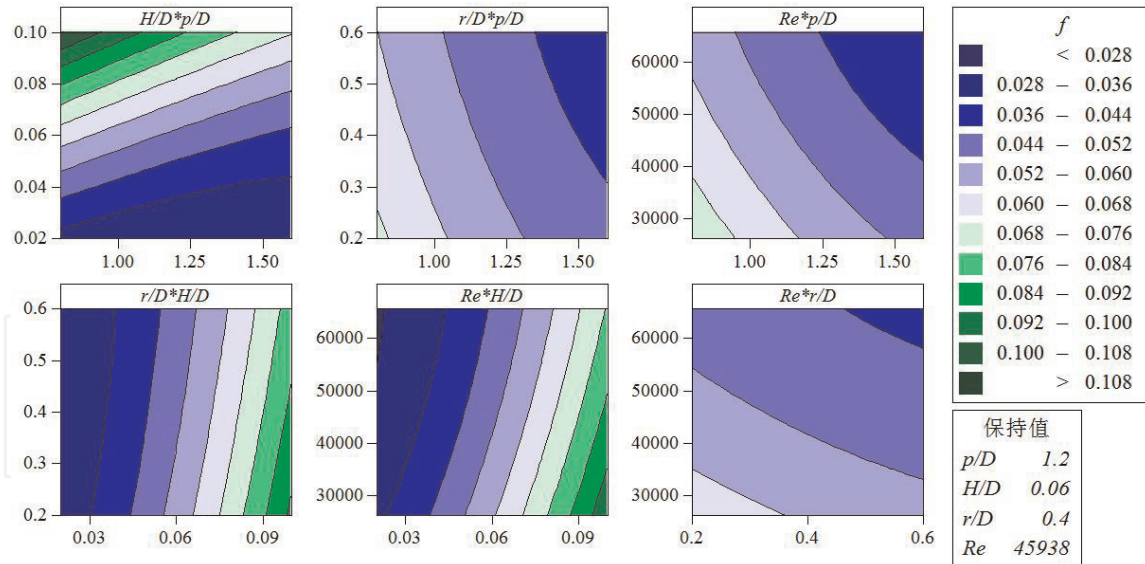
Figure 22.
Response surfaces contour plots of combined effects for f_c.

can be observed that the decrease of p/D, the increase of H/D, the decrease of r/D, and the increase of Re result in the augment of Nu. Moreover, it can be also seen that the decrease of p/D, the decrease of H/D, the increase of r/D, and the decrease of Re result in the weak of f_c.

5.5 Pareto front

By inspecting the numerical results of Nu_c/Nu_s and f_c/f_s, it is found that these two responses are varied with the changes of the design parameters. There must exist design parameters corresponding to the optimal objective functions. The goal of optimization for a corrugated tube subjected the design constrains of structural limitation in this study is to find the optimal values of designing parameters to maximize Nu_c/Nu_s and minimize f_c/f_s. In this study, the multi-objective optimization is executed by NSGA-II. The results for Pareto-optimal curve are shown in **Figure 23**, which clearly reveal the conflict between the two responses, Nu_c/Nu_s and f_c/f_s. Any changed design parameter that increases Nu_c/Nu_s leads to an increase of f_c/f_s. It is worth noting that the minimum values of f_c/f_s with Nu_c/Nu_s for various points on Pareto optimal front. Therefore, the reported results are applicable for a problem with one objective function (f_c/f_s) and specific constraint (the value of
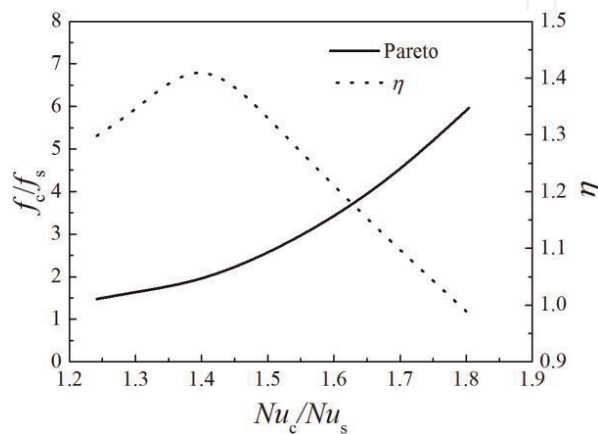

Figure 23.
Pareto-optimal curve.

selected or input Nu_c/Nu_s). This means that the presented multi-objective optimization method provides a general optimal solution in simplified form, and one may obtain an optimum design (minimum of f_c/f_s and maximum of η) with a specified Nu_c/Nu_s.

6. Conclusions

A deep investigation of the heat and mass transfer was given in outward convex corrugated tube heat exchangers in this chapter. The detailed structure of the novel tube has been introduced, in which the heat and mass transfer mechanism is different with the traditional tube type. A specific manufacturing procedure by hydraulic bulking system has been presented for the novel tube type. The experimental setup and measuring system for the novel tube type have been depicted. From obtained experimental data, we found that with the increase of Re, Nu_c/Nu_s, f_c/f_s, and PEC decline. The decreasing rate of Nu_c/Nu_s and PEC is almost linear, but f_c/f_s is decelerated. The numerical study on the heat and mass transfer at outward convex corrugated tube heat exchangers has been displayed. The distribution of velocity, temperature, and turbulence kinetic energy has been analyzed. The recirculating zone between the separating streamline and the free boundary streamline is generated, which breaks the thermal boundary layer to enhance the heat transfer performance. Turbulence kinetic energy is improved at the recirculating zone. Heat and mass transfer enhancement of outward convex corrugated tube heat exchangers has been revealed. Both on the tube side and shell side, with the decreasing p/D and increasing H/D, the values of Nu_c and Nu_c/Nu_s increase. Moreover, with the increase of p/D, η decreases when $Re < 30,000$, but increases when $Re > 30,000$; the η decreases obviously with the increasing H/D. The multi-objective optimization is executed by RSM combined with NSGA-II. ANOVA is used to evaluate the fitness of regression models, perform significance testing, and construct simplified regression models between design factors and objective functions. 2D response surface contour plots are applied to describe the regression response surface model. Multi-objective optimization method provides a general optimal solution in simplified form, and one may obtain an optimum design (minimum of f_c/f_s and maximum of η) with a specified Nu_c/Nu_s.

Acknowledgements

Conflict of interest

The article has not been previously published, is not currently submitted for review to any other journal, and will not be submitted elsewhere before one decision is made.

Author details

Huaizhi Han[1,2*], Bingxi Li[3], Yaning Zhang[3], Quan Zhu[1] and Ruitian Yu[2]

1 School of Chemical Engineering, Sichuan University, Chengdu, China

2 College of Power and Energy Engineering, Harbin Engineering University, Harbin, China

3 School of Energy Science and Engineering, Harbin Institute of Technology, Harbin, China

*Address all correspondence to: hanhz_hrbeu@163.com

IntechOpen

References

[1] Han HZ, Li BX*, Yu BY, He YR, Li FC. Mint: Numerical study of flow and heat transfer characteristics in outward convex corrugated tubes. International Journal of Heat and Mass Transfer. 2012;**55**:7782-7802. DOI: 10.1016/j.ijheatmasstransfer.2012.08.007

[2] Yang LB, Han HZ*, Li YJ, Li XM. Mint: A numerical study of the flow and heat transfer characteristics of outward convex corrugated tubes with twisted-tape insert. ASME Journal of Heat Transfer. 2016;**138**:1-8. DOI: 10.1115/1.4031171

[3] Wang FQ, Tang ZX, Gong XT, Tan JY*, Han HZ, Li BX. Mint: Heat transfer performance enhancement and thermal strain restrain of tube receiver for parabolic trough solar collector by using asymmetric outward convex corrugated tube. Energy. 2016;**114**:275-295. DOI: 10.1016/j.energy.2016.08.013

[4] Wang FQ, Lai QZ, Han HZ, JY T. Mint: Parabolic trough receiver with corrugated tube for improving heat transfer and thermal deformation characteristics. Applied Energy. 2016;**164**:411-424. DOI: 10.1016/j.apenergy.2015.11.084

[5] Gong XT, Wang FQ, Wang HY, Tan JY, Lai QZ, Han HZ. Mint: Heat transfer enhancement analysis of tube receiver for parabolic trough solar collector with pin fin arrays inserting. Solar Energy. 2017;**144**:185-202. DOI: 10.1016/j.solener.2017.01.020

[6] Han HZ, Li BX*, Shao W. Mint: Effect of flow direction for flow and heat transfer characteristics inoutward convex a symmetrical corrugated tubes. International Journal of Heat and Mass Transfer. 2016;**92**:1236-1251. DOI: 10.1016/j.ijheatmasstransfer.2014.11.076

[7] Han HZ, Yu RT, Li BX, Zhang YN, Wang W. Mint: Multi-objective optimization of corrugated tube with loose fit twisted tape using RSM and NSGA-II. International Journal of Heat and Mass Transfer. 2019;**131**:781-794. DOI: 10.1016/j.ijheatmasstransfer.2018.10.128

[8] Han HZ, Li BX*, Wu H, Shao W. Mint: Multi-objective shape optimization of double pipe heat exchanger with inner corrugated tube using RSM method. International Journal of Thermal Sciences. 2015;**90**:173-186. DOI: 10.1016/j.ijthermalsci.2014.12.010

[9] Han HZ, Li BX*, Shao W. Mint: Multi-objective optimization of outward convex corrugated tubes using response surface methodology. Applied Thermal Engineering. 2014;**70**:250-262. DOI: 10.1016/j.applthermaleng.2014.05.016.

[10] Shah RK, Sekulić Dušan P. Surface basic heat transfer and flow friction characteristics. In: R K S, Sekulić Dušan P, editors. Fundamentals of Heat Exchanger Design. Hoboken: John Wiley & Sons; 2017. pp. 425-562. DOI: 10.1002/9780470172605.ch7

[11] Karthikeyan D. Thermal analysis of Shell and tube heat exchanger using CFD. In: Parmar N, editor. Design and Analysis Shell and Tube Type Heat Exchanger: Taguchi Method and CFD Analysis. Balti: LAG LAMBERT Academic Publishing; 2017. pp. 26-43. DOI: 110.5281/zenodo.56040

[12] Russell TF, Robinson AS, Wagner NJ, editors. Mass and Heat Transfer: Analysis of Mass Contactors and Heat Exchangers. New York: Cambridge University Press; 2008

[13] ANSYS FLUENT User's Guide, Release 17.0. Ansys Inc.; 2016